Electron transport across a metal-organic interface: Simulations using nonequilibrium Green's function and density functional theory

Kurt Stokbro[*] and Søren Smidstrup[†]

QuantumWise A/S, Lersø Parkallé 107, DK-2100 Copenhagen, Denmark[‡]

We simulate the electron transport across the Au(111)-pentacene interface using nonequilibrium Green's functions and density-functional theory (NEGF-DFT), and calculate the bias-dependent electron transmission. We find that the electrical contact resistance is dominated by the formation of a Schottky barrier at the interface, and show that the conventional semiconductor transport models across Schottky barriers need to be modified in order to describe the simulation data. We present an extension of the conventional Schottky barrier transport model, which can describe our simulation results and rationalize recent experimental data.

I. INTRODUCTION

Organic materials for electronics is a rapidly growing area, with new commercial organic devices for applications in lighting, displays, and photovoltaics being considered. An important problem is the control of charge injection at the metal-organic interface. The charge injection can be associated with a large contact resistance, and is sometimes more dominating for the electrical performance than the transport within the organic material. The transport across the interface is usually described by the theory of metal-semiconductor contacts,[1–4] where the transport is characterized by an injection barrier that needs to be overcome by thermionic emission.[5] In this paper we show that this theory cannot explain first-principles data of quantum transport across a metal-organic interface. Organic crystals have much narrower electron bands than "traditional" inorganic semiconductors, and the theory must be extended to take into account that for certain electron injection energies there may be no available organic crystal bands in the band bending region, and the electron needs to tunnel through this region.

Previous theoretical studies of the metal-organic interface have focused on understanding the properties of a single or few layers of organic molecules on metal surfaces. The focus in this paper is to simulate a true interface between a gold and a pentacene bulk crystal through the use of density-functional theory (DFT) and the nonequilibrium Green's function (NEGF) method. To our knowledge this is the first study of a single metal-organic interface which does not make use of a slab geometry, but models semi-infinite electrodes by applying open boundary conditions. We show how such simulations can give new insight into the electrostatic properties of the interface, the contact resistance, and electron transport across the interface.

We have chosen the gold-pentacene crystal interface as our model system. Due to its high hole mobility, the pentacene crystal is an important organic electronic material, and the gold-pentacene interface is one of the most well studied systems both theoretically[6–11] and experimentally,[4,12–22] thus there is a large number of experimental and theoretical data for verification of the theoretical simulations.

The organization of the paper is the following. In Sec. II we describe the computational model used for the calculations, and in Sec. III we present the results of the calculations.

Section IV presents a simple model which rationalize the results and the results are summarized in Sec. V.

II. METHODOLOGY

For all calculations we have used Atomistix ToolKit (ATK),[23] which is a density-functional theory code that uses numerical localized atom centered basis sets and norm conserving pseudopotentials. For the exchange-correlation potential we have used the generalized gradient approximation (GGA) of Wang and Perdew[24] (PW91) as suggested by Li *et al.*[7]

The electronic structure is expanded in basis sets optimized to reproduce hydrogen and carbon dimer total energies following the procedure of Blum *et al.*[25] For carbon we use 21 orbitals per atom with s, p, and d character and radial ranges up to 3.9 Å, and for hydrogen we use 5 orbitals per atom with s and p character and ranges up to 4.2 Å. For gold we use a minimal basis set with 9 orbitals per atom and ranges up to 3.6 Å, and add a layer of gold ghost orbitals above the gold surface. With this model we calculate an ionization energy of 6.34 eV (6.589[26]) for pentacene, and a work function of 5.20 eV (5.26[27]) for the Au(111) surface, where the corresponding experimental values are given in parentheses.

To describe the gold-pentacene interface we correct for basis set superposition errors (BSSE) in the interaction between gold and pentacene. This is done using the counterpoise correction dividing the system into gold surface (including ghost atoms) and the pentacene overlayers.[8] Similar to previous studies, we use an (8×3) k-point grid,[7] and with this model we reproduce the geometry, work function change, and adsorption energy[28] of pentacene on the Au(111)-($\sqrt{3} \times 6$) surface obtained with a plane-wave method.[7,28] In this paper we study pentacene on the Au(111)-($2 \times 3\sqrt{3}$) surface. This structure has been observed experimentally[12] and the adsorption energy of a pentacene monolayer is higher for this structure compared with the Au(111)-($\sqrt{3} \times 6$) surface.[28]

III. RESULTS

The experimentally observed pentacene crystal geometry[29] is shown in Fig. 1(b). To combine the crystal with the Au(111)-($2 \times 3\sqrt{3}$) cell, it is necessary to strain the pentacene crystal
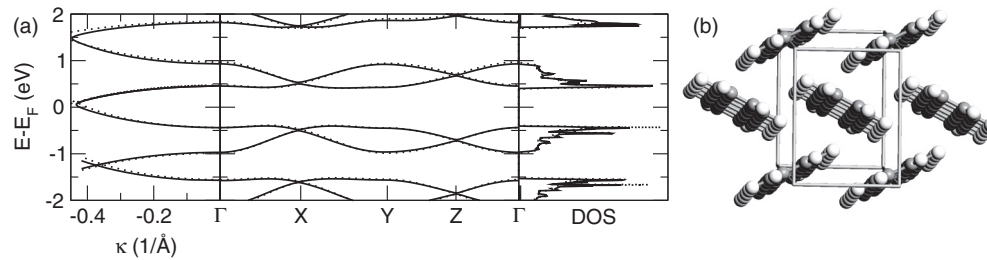
FIG. 1. The solid lines show the complex band structure, band structure, and DOS of the relaxed pentacene crystal. The dotted lines show the corresponding values for the strained crystal which is used for the right electrode of the Au(111)-pentacene interface configuration.

$\sim$3% in the interface plane. With this constraint on the cell, we then optimize the length of the interface cell in the transport direction and the pentacene coordinates. To investigate the influence of such modifications on the electronic structure we have calculated the complex band structure, band structure, and density of states of the pentacene crystal at the experimental lattice constant and compared them with the strained crystal. The results are shown in Fig. 1(a), where the dotted lines are for the strained case. We see that the electronic structure is almost identical to the unstrained pentacene crystal (solid lines), and thus the straining of the crystal will only have a minor impact on our electron transport calculations.

To set up the geometry of the Au(111)-pentacene interface, we have first relaxed an Au(111)-($2 \times 3\sqrt{3}$) slab with two pentacene layers, until the forces of all pentacene atoms and the first two gold layers were below 0.01 eV/Å. We next used the pentacene crystal as a template for extending the slab from two to six pentacene layers, and relaxed all atoms in layers 2, 3, and 4 until the forces were below 0.02 eV/Å. Finally, we attached semi-infinite electrodes to set up a device configuration as shown in Fig. 2. The BSSE correction cannot be applied in the device configuration, and we can therefore only obtain reliable forces for atoms in pentacene layers 2, 3, and 4. In these layers the forces are below 0.04 eV/Å, confirming that our procedure for generating the geometry using a slab configuration is accurate. In the following we will calculate the properties of this interface.

Figure 2(c) shows the local density of states (LDOS) of the Au(111)-pentacene interface plotted along the transport direction z. The five gold layers and six pentacene layers are visible as z positions with large LDOS values. For the pentacene layers we clearly see the molecular levels. We note the shifts in the molecular levels in the z direction, corresponding to a band bending in the organic crystal at the interface. The solid white line shows the average electrostatic potential, which exhibits the same band bending behavior.

Figure 2(c) also shows how the metallic gold states extend through the adsorbed pentacene molecules into the pentacene crystal. This is seen as an asymmetric shape of the LDOS states, with a long tail at energies above the maximum in the LDOS peak. This is particularly clear for molecules in the third layer above the interface. Thus, the LDOS illustrates the difficulties for the metallic states to propagate through the band bending region into the pentacene electrode.

The band bending is a result of Fermi level pinning of the pentacene highest occupied molecular orbital (HOMO) at the

gold-pentacene interface, which shifts the pentacene levels at the interface relative to their positions in the organic crystal electrode. The electronic structure in this (the right) electrode is that of an intrinsic pentacene bulk crystal (charge neutral) and the charge neutrality condition gives a Fermi level in the middle
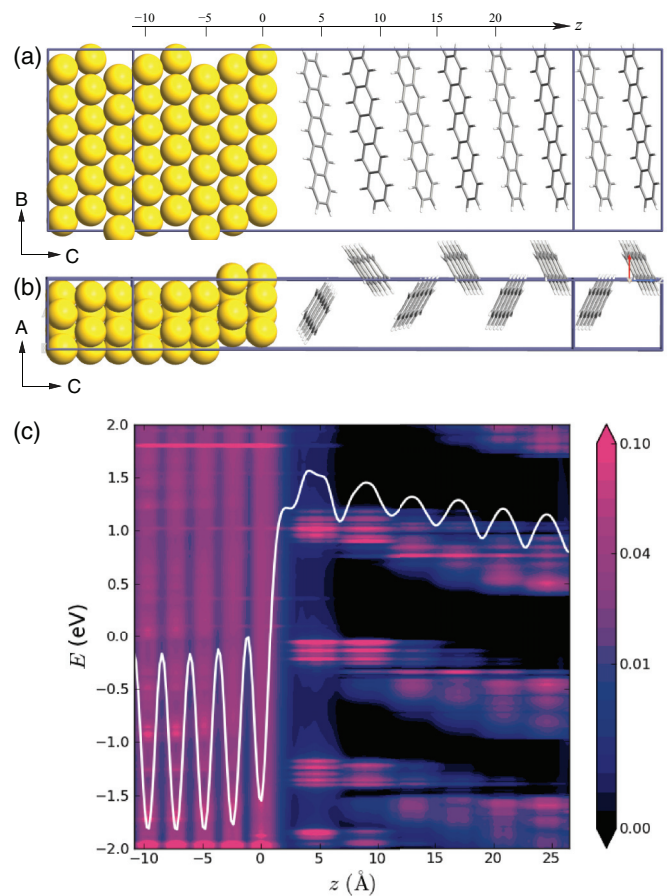

FIG. 2. (Color online) In our notation, the Au(111)-pentacene interface is spanned by the crystal cell vectors $A||x$ and $B||y$, while the transport direction is $C||z$. Side views of the (a) BC and the (b) AC planes of the interface are shown here. The outermost parts show the geometry of the semi-infinite electrodes. (c) Contour plot of the local density of states (LDOS) of the Au-pentacene interface and the electrostatic potential (white line) along the z direction. The energy E is given relative to the electrode Fermi levels (which coincide at zero bias), and the LDOS and the potential are averaged over the xy plane. An (8×3) k-point grid was used for the LDOS calculation.
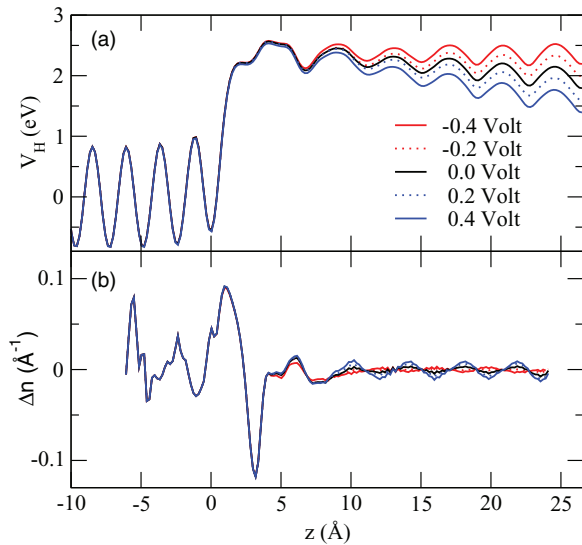
FIG. 3. (Color online) (a) Electrostatic potential of the gold-pentacene interface averaged over the xy plane for right electrode voltages $U_R = -0.4, -0.2, 0.0, 0.2$, and 0.4 V. (b) Change in electron density upon adsorption of pentacene on gold, i.e., the electron density of the isolated gold surface and the isolated pentacene crystal are subtracted from the combined system. The density is integrated over the xy plane, and shown for the same bias voltages as (a).

of the band gap. When no bias is applied between the two electrodes, the gold and pentacene Fermi levels are aligned, and the pentacene HOMO band edge in the right electrode is ~0.4 eV below the gold Fermi level. At the interface the HOMO is pinned to the gold Fermi level, creating a total band bending of 0.4 eV.

It is the charge neutrality condition for the electrode which in our calculation gives rise to the band bending, and for an n-doped pentacene electrode the band bending will be larger, while it will be very small or vanishing for a p-doped pentacene electrode at zero bias. Thus, it is the boundary condition which determines the band bending, and for a larger central region the band bending will take place over a larger distance. In a real system the size of the band bending region will depend on the doping level of the organic crystal and is typically several orders of magnitude larger than in our calculation. Thus, this

is a basic limitation of the calculation which must be kept in mind when comparing the modeling results with experimental data.

The pinning of the HOMO level arises because the ionization energy of the pentacene crystal is lower than the work function of the gold surface. We calculate a work function of gold of 5.20 eV and an ionization energy of the pentacene crystal of 5.04 eV.

Figure 3(b) shows the change in the electron density of the gold interface upon adsorption of pentacene. The plot was obtained by subtracting the electron density of the isolated gold and pentacene surfaces from the combined system, and shows the formation of a surface dipole at the interface. Note that this is not a charge transfer from pentacene to gold, since the dipole is located between the top gold layer and the first pentacene layer. The surface dipole arises from the so-called pillow effect,[30] where the pentacene molecule pushes the gold density back.

This surface dipole lowers the work function of gold. For a single layer of pentacene on Au(111) we calculate a work function of 4.48 eV,[28] which is in excellent agreement with experimental data (4.52,[14] 4.4,[18] and 4.6[21] eV). When adding more pentacene layers, the work function will be lowered due to the band bending. For two pentacene layers we calculate a work function of 4.44 eV.

We next apply different bias voltages, $U_R = -0.4, -0.2, 0.0, 0.2$, and 0.4 V to the pentacene electrode. The bias will shift the electrochemical potential in the organic electrode by $\mu_R = \mu_L - eU_R$ relative to the chemical potential μ_L in the metal electrode. Figure 3(a) shows the electrostatic potential along the z direction for the different bias voltages. The zero-bias potential corresponds to the electrostatic potential of Fig. 2(c). A negative bias increases the pentacene electrochemical potential μ_R and thereby reduces the band bending, while a positive bias lowers μ_R which increases the band bending.

Figure 4(a) shows the calculated current-voltage characteristics of the interface. The interface shows a strong rectifying behavior. The inset in the figure also shows the temperature dependence of the current. The temperature dependence shows activated electron transport, meaning that thermionic emission is the dominating current contribution. For each bias the barrier corresponding to the slope of the curve is
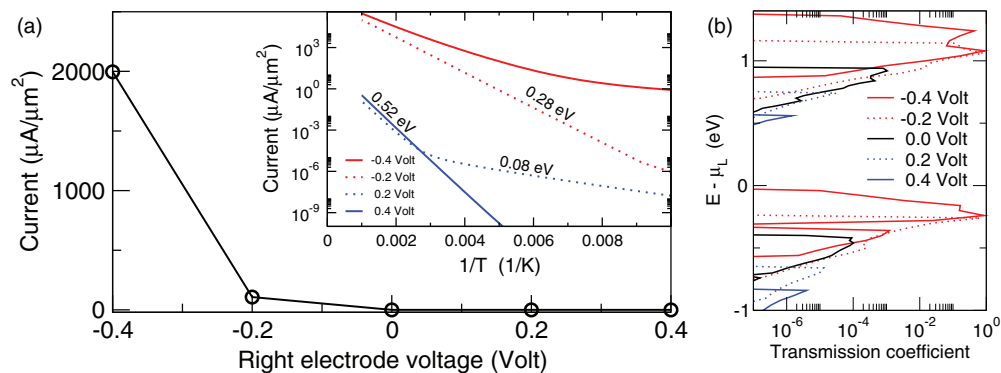

FIG. 4. (Color online) (a) Current-voltage characteristics of the gold-pentacene interface. The inset shows the temperature dependence of the current at each bias voltage. (b) Transmission spectra for each bias voltage. The transmission spectra are averaged over an (8×3) k-point grid, and the the energy scale is relative to the left electrochemical potential μ_L.

indicated. In the following we will investigate this in further detail and make a simple model of the transport across the interface.

Figure 4(b) shows the transmission spectrum as function of the bias voltage applied to the right electrode. The transmission increases exponentially when a negative voltage is applied. At −0.4 V the maximum transmission is 1, corresponding to a very good coupling between the pentacene crystal and the gold electrode. It follows from the discussion of the band bending above that the system is in flat band condition at this bias voltage, which can also be seen in Fig. 3. For the other computed bias points the bands bend downwards, and a Schottky-type barrier arises at the interface.

In an inorganic semiconductor, a Schottky barrier is reflected by an energy shift of the transmission peaks relative to the metal Fermi level; however, the magnitude of the transmission peaks will not change. For the pentacene crystal, the transmission peaks are both shifted and reduced in magnitude. The reduction is an effect of the band bending of the narrow molecular bands. The band bending is of similar magnitude as the widths of the organic bands, which has the effect that the electron cannot propagate inside a molecular band all the way from the organic crystal to the metal electrode. Outside a molecular band the wave function amplitude is exponentially damped with the tunneling distance, thus, for increasing band bending the transmission peak is exponentially lowered.

IV. DISCUSSION

Finally, we present a model that quantifies the reduction of the transmission peaks in the inorganic crystal due to the tunneling through the band bending region. Figure 5 shows the transmission averaged over the HOMO and the LUMO peaks. The curve is flat up to −0.2 V, and then decreases exponentially. The dashed black line shows a WKB model of the transmission, where the average transmission is given by

$$T \propto e^{-2d\sqrt{\frac{2m}{\hbar^2}\bar{\phi}}}. \tag{1}$$

In this equation $d = 23$ Å is the distance from the first pentacene layer to the right electrode, and $\bar{\phi} = \frac{1}{2}e(U_R - U_0)$ is an effective tunnel barrier, corresponding to vanishing barrier at $U_0 = -0.2$ V and a linearly increasing barrier $e(U_R - U_0)z/d$ as a function of z.
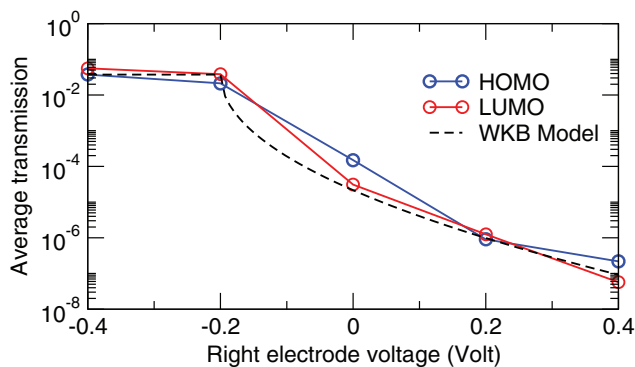
FIG. 5. (Color online) The average transmission of the HOMO (blue line) and the LUMO (red line) transmission peaks. A simple WKB model of the transmission is shown as the dashed line.
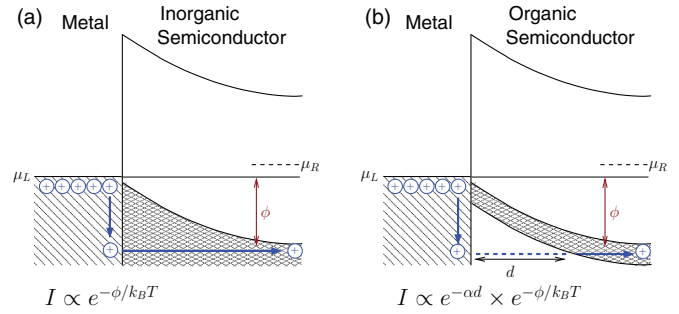
FIG. 6. (Color online) Band diagram of a Schottky barrier under forward bias for (a) metal-inorganic semiconductor and (b) metal-organic semiconductor interface. The semiconductor is intrinsic with the Fermi level in the middle of the band gap. Under forward bias a negative voltage is applied to the semiconductor and it drives a thermionic hole current from the metal to the semiconductor. Due to the finite width of the organic crystal bands, the electron transmission is exponentially damped when propagating over the Schottky barrier of the metal-organic interface.

The total current at bias $eU_R = \mu_L - \mu_R$ is given by

$$I \propto \int T(E)\left[f\left(\frac{E-\mu_L}{k_BT}\right) - f\left(\frac{E-\mu_R}{k_BT}\right)\right]dE, \tag{2}$$

where $T(E)$ is the transmission coefficient, f is the Fermi function, T is the electron temperature, and k_B is the Boltzmann constant.

Under forward bias the current can be approximated by

$$I \propto T(E_v)e^{-\phi/k_BT}, \tag{3}$$

where $E_v = \mu_L - \phi$ and ϕ is the offset between the semiconductor valence band and the metal chemical potential. For an inorganic semiconductor $T(E_v) \sim 1$, but for an organic semiconductor $T(E_v) \sim e^{-\alpha d}$ as inferred from Eq. (1).

This qualitative difference in the electron transmission across a metal-semiconductor interface for inorganic and organic systems, respectively, is illustrated in Fig. 6. The figures model a Schottky barrier between a metal and an intrinsic (or lightly p-doped) semiconductor. At forward bias (negative voltage at the semiconductor) a thermionic hole current will run from the metal to the semiconductor. For the inorganic system the current will be given by the number of carriers thermally excited over the Schottky barrier. For the organic crystal, the narrow organic crystal bands leads to an additional contact resistance, since in this case the thermally excited carriers need to tunnel through part of the band bending region.

It is interesting to compare this model with the experimental data for transport across the gold-pentacene interface by Liu et al.[4] They find a large contact resistance and rectification for the gold-pentacene interface, in qualitative agreement with our calculations. A quantitative comparison is not immediately possible since the effective contact area is unknown in the experiment, and a discussed previously the size of the band bending region is too small in the simulation. Liu et al. model the data in terms of a traditional Schottky barrier. In order to explain the large contact resistance they suggest that the interface dipole rigidly shifts the bands in the organic semiconductor, which introduces an additional injection barrier. We

note, however, that their model assumes a shift of the Fermi level in the organic crystal relative to its HOMO and LUMO bands upon forming the interface with gold, thus, the interface dipole should change the organic crystal from *p* to *n* type, which we find unphysical.

Liu *et al.* also assume band bending at the interface, however, in their case the band bending has no direct electrical effect on the contact resistance. Our model suggests that the band bending will indeed affect the injection probability, thus leading to an alternative model for the large contact resistance which does not require the introduction of an additional injection barrier.

Furthermore, Liu *et al.* noticed that the metal-organic contact resistance can be reduced by incorporating an inorganic semiconductor buffer layer between the metal and the organic crystal.[3,4] They suggest that the effect of the inorganic semiconductor is to remove the interface dipole and thereby the additional injection barrier. We propose an alternative explanation for this effect. The buffer layer will unpin the HOMO band at the interface, making the organic crystal bands more flat, which increases the electron propagation probability in the band bending region. Thus, unlike models proposed previously,[3,4] we suggest that the buffer layers will not change the Schottky barrier, but rather increases the injection probability due to flatter inorganic bands which provides more efficient propagation through the band bending region.

V. SUMMARY

In summary, we have studied bias-induced electron transport across the Au(111)-pentacene interface. The study shows that there is a good chemical contact between the gold and the pentacene crystals, and the electrical resistance is dominated by a Schottky barrier within the organic crystal. The transport across the Schottky barrier is thermally activated, however transport is reduced compared to an inorganic semiconductor, since the electron needs to tunnel through part of the band bending region, as illustrated in Fig. 6. Our calculation is a simplification compared to an experimental situation; in particular, the length of the band bending region is orders of magnitude shorter than it is experimentally. However, the calculations suggest an overlooked effect, namely that propagation through the band bending region can be damped due to the narrow bands in the organic material. We have illustrated how such a model can rationalize recent experimental data for the contact resistance of the gold-pentacene interface and explain the effect of an inorganic buffer layer on the contact resistance.

*kurt.stokbro@quantumwise.com

†soren.smidstrup@quantumwise.com

‡http://quantumwise.com

[1]H. Ishii, K. Sugiyama, E. Ito, and K. Seki, Adv. Mater. **11**, 605 (1999).

[2]S. Braun, W. R. Salaneck, and M. Fahlman, Adv. Mater. **21**, 1450 (2009).

[3]A. Kumatani, P. Dermawan, T. Minari, and K. Tsukagoshi, Sci. Rep. **3**, 1026 (2013).

[4]Z. Liu, M. Kobayashi, B. C. Paul, Z. Bao, and Y. Nishi, Phys. Rev. B **82**, 035311 (2010).

[5]S. M. Sze, *Physics of Semiconductor Devices* (Wiley, New York, 1981).

[6]B. Pieczyrak, E. Abad, F. Flores, and J. Ortega, J. Chem. Phys. **135**, 084702 (2011).

[7]H. Li, Y. Duan, V. Coropceanu, and J.-L. Bredas, Organic Electron. **10**, 1571 (2009).

[8]K. Lee, J. Yu, and Y. Morikawa, Phys. Rev. B **75**, 045402 (2007).

[9]K. Lee and J. Yu, Surf. Sci. **589**, 8 (2005).

[10]K. Toyoda, I. Hamada, K. Lee, S. Yanagisawa, and Y. Morikawa, J. Chem. Phys. **132**, 134703 (2010).

[11]G. Saranyaa, S. N. V. Natarajanb, P. Kolandaivela, and K. Senthilkumara, J. Mol. Graphics Model. **38**, 334 (2012).

[12]N. Koch, A. Kahn, J. Ghijsen, J. Pireaus, J. Schwartz, R. L. Johnson, and A. Elschner, Appl. Phys. Lett. **82**, 70 (2007).

[13]O. McDonald, A. A. Cafolla, D. Carty, G. Sheerin, and G. Hughes, Surf. Sci. **600**, 3217 (2006).

[14]P. Schroeder, C. B. France, J. B. Park, and B. A. Parkinson, J. Appl. Phys. **91**, 3010 (2002).

[15]K. Ihm, B. Kim, T.-H. Kang, K. Kim, M. H. Joo, T. H. Kim, S. S. Yoon, and S. Chung, Appl. Phys. Lett. **89**, 033504 (2006).

[16]C. B. France, P. Schroeder, J. B. Forsythe, and B. A. Parkinson, Langmuir **19**, 1274 (2003).

[17]D. Käfer, L. Ruppel, and G. Witte, Phys. Rev. B **75**, 085309 (2007).

[18]N. J. Watkins, L. Yan, and Y. Gao, Appl. Phys. Lett. **80**, 4384 (2002).

[19]J. H. Kang and X.-Y. Zhu, Appl. Phys. Lett. **82**, 3248 (2003).

[20]W.-H. Soe, C. Manzano, A. De Sarkar, N. Chandrasekhar, and C. Joachim, Phys. Rev. Lett. **102**, 176102 (2009).

[21]L. Diao, C. D. Frisbie, D. D. Schroepfer, and P. P. Ruden, J. Appl. Phys. **101**, 014510 (2007).

[22]J. Park and J. S. Choi, Synth. Met. **155**, 657 (2005).

[23]The calculations where performed with Atomistix ToolKit, version ATK-12.8, QuantumWise A/S (2012), http://quantumwise.com/documents/manuals.

[24]Y. Wang and J. P. Perdew, Phys. Rev. B **43**, 8911 (1991).

[25]V. Blum, R. Gehrke, F. Hanke, P. Havu, X. Ren, K. Reuter, and M. Scheffler, Comput. Phys. Commun. **180**, 2175 (2009).

[26]N. E. Gruhn, D. A. da Silva Filho, T. G. Bill, M. Malagoli, V. Coropceanu, A. Kahn, and J.-L. Brédas, J. Am. Chem. Soc. **124**, 7918 (2002).

[27]G. V. Hansson and S. A. Flodström, Phys. Rev. B **18**, 1572 (1978).

[28]K. Stokbro and S. Smidstrup, arXiv:1308.0969.

[29]S. Schiefer, M. Huth, A. Dobrinevski, and B. Nickel, J. Am. Chem. Soc. **129**, 10316 (2007).

[30]N. Koch, A. Volmer, S. Duhm, Y. Sakamoto, and T. Suzuki, Adv. Mater. **19**, 112 (2007).